Journal of Solid State Chemistry **152,** 340–347 (2000)
doi:10.1006/jssc.2000.8658, available online at http://www.idealibrary.com on IDEAL®

Order–Disorder and Mobility of Li^+ in the β'- and β-$LiZr_2(PO_4)_3$ Ionic Conductors: A Neutron Diffraction Study

M. Catti,* N. Morgante,* and R. M. Ibberson†

*Dipartimento di Scienza dei Materiali, Università di Milano Bicocca, via Cozzi 53, 20125 Milano, Italy; and †ISIS Facility, CLRC Rutherford Appleton Laboratory, Chilton, Didcot, Oxon OX11 0QX, United Kingdom

Received November 17, 1999; in revised form February 8, 2000; accepted February 18, 2000

Neutron diffraction profiles at high resolution (HRPD, ISIS Facility, U.K.) were collected on powder samples of $LiZr_2(PO_4)_3$ at 20°C (β'phase, monoclinic $P2_1/n$, $Z=4$; $a=8.81277(4)$, $b=8.94520(5)$, $c=12.37540(6)$ Å, $\beta=90.801(1)^\circ$) and at 350°C (β phase, orthorhombic $Pbna$, $Z=4$; $a=8.84303(5)$, $b=8.94120(6)$, $c=12.41301(8)$ Å). All Li sites were located by difference Fourier maps in tetrahedral coordination, and both structures were Rietveld-refined to $wR_p=0.0353$ (β') and 0.0429 (β). The β' structure is a distortion of β, with a [100] pseudo-twofold axis x, $1/2-y$, $-z$ relating all atoms but lithium, which is fully ordered ($\langle$Li–O$\rangle=2.02$ Å). In the β phase, Li is disordered over four sites, of which two (Li1 and Li2) are symmetry-independent with occupancies 0.34(1) and 0.16(1), respectively, and $\langle$Li–O$\rangle=2.17$ and 2.16 Å. The disorder fully explains the higher Li^+ mobility in the β with respect to the β' phase observed from ionic conductivity data. Mechanisms of ion transport are proposed, and the relationship to the NASICON-type α'/α phase of $LiZr_2(PO_4)_3$ is analyzed in detail. © 2000 Academic Press

Key Words: **neutron diffraction; Rietveld refinement; ionic conductivity; $LiZr_2(PO_4)_3$.**

INTRODUCTION

Within the large family of $AM_2(XO_4)_3$ ionic conductors with NASICON-related crystal structures, $LiZr_2(PO_4)_3$ has long been known to be one of the compounds displaying the most complex polymorphism (1–4). As the ionic conductivity behavior is usually different for every crystalline modification, this system is potentially a rich source of data connecting Li^+ ion mobility and structural features, so as to provide challenging tests for models of ionic transport mechanisms. Only a full understanding of the atomistic basis for ionic conduction would allow us to design new materials with superior performances as solid electrolytes (5, 6), cathodes for rechargeable batteries (7), and electrochemical gas sensors (8).

When prepared by solid state reaction at 1200°C, $LiZr_2(PO_4)_3$ forms the rhombohedral NASICON structure (α phase, space group $R\bar{3}c$), which is stable at $T>60$°C, while on cooling it transforms to the distorted triclinic α' phase ($C\bar{1}$). If, on the other hand, the synthesis is carried out at a lower temperature (below 900°C), then $LiZr_2(PO_4)_3$ crystallizes in the orthorhombic β-$Fe_2(SO_4)_3$-type structure (β phase, $Pbna$), which at $T<300$°C transforms into the distorted monoclinic β' phase ($P2_1/n$). Both the $\alpha'\leftrightarrow\alpha$ and $\beta'\leftrightarrow\beta$ phase transitions are fully reversible, so that the high-temperature modifications cannot be quenched. No direct transformations between the α- and β-type phases have been observed so far.

The ionic conductivity measurements (1) at $T=300°C$ gave $\sigma\sim10^{-2}$ and $5\times10^{-4}\,\Omega^{-1}\,cm^{-1}$ for the α and β phases of $LiZr_2(PO_4)_3$, respectively, so that there is a gain of over an order of magnitude of σ on passing from β to α. The corresponding activation energies are 0.42 (α) and 0.28 (β) eV. Much lower conductivities are shown by the low-temperature distorted α' and β' phases. In particular, the latter phase has $\sigma\sim10^{-10}\,\Omega^{-1}\,cm^{-1}$ at room temperature, but shows a large activation energy of 0.91 eV, which produces a very significant conductivity increase with temperataure. There is thus clearly a need to explain this huge jump of activation energy, from 0.91 to 0.28 eV, across the $\beta'\rightarrow\beta$ phase transition at $T\sim300$°C. This requires an accurate location of the Li atoms within the corresponding structures, and the high-resolution powder neutron diffraction technique has proved to be very efficient in this respect. Indeed, by this method we were recently able to solve similar problems on the α' and α phases of $LiZr_2(PO_4)_3$, by fully explaining the large conductivity increase from α' and α on structural grounds (3, 4).

We have thus undertaken a study of the crystal structures of β'- and β-$LiZr_2(PO_4)_3$ at room temperature and 350°C, respectively, with the primary goals of determining the crystal-chemical environment of lithium atoms in both phases and of relating it to the ionic conductivity behavior. In fact, it is expected that the $\beta'\leftrightarrow\beta$ transition might have an order–disorder character, and that would be the key to explain the corresponding jump of activation energy observed in the

0022-4596/00 $35.00

Arrhenius plot. We also aim to clarify the connection between lithium locations in the β/β' and α/α' structural types, in order to account for the lower Li^+ mobility observed in the first with respect to the second case.

EXPERIMENTAL

The synthesis of β'-$LiZr_2(PO_4)_3$ (F.W. = 474.29) was carried out by solid state reaction (1). Reagent-grade Li_2CO_3, ZrO_2, and $NH_4H_2PO_4$ were mixed in stoichiometric ratios in a Pt boat and heated for 1 h at 500°C, then for 20 h at 800°C in a tubular furnace. The sample obtained was ground, pelletized, and again heated at 800°C for 18 h. Powder X-ray diffractometry (Siemens D500 apparatus, Cu$K\alpha$ radiation) proved the product to be pure monoclinic β' phase, but for the presence of a small quantity of ZrP_2O_7, which could not be removed by further thermal treatments; no traces were found of the triclinic α' phase, obtained at higher temperature. The transition to the orthorhombic β phase was confirmed to occur reversibly at about 300°C both by differential thermal analysis (Perkin–Elmer DTA 1600) and by high-temperature powder X-ray diffraction (Buehler HT-attachement to the D500 diffractometer).

Neutron diffraction data were collected on the time-of-flight high-resolution powder diffractometer (HRPD), equipped with a furnace, at the ISIS spallation pulsed source, Rutherford Appleton Laboratory (Chilton, U.K.). The 2-cm^3 sample was contained in a vanadium can under vacuum. By use of the back-scattering counter bank at $\langle 2\theta \rangle = 168.3°$, full intensity profiles were recorded in the d_{hkl} range 0.9 to 2.5 Å (with an instrumental resolution of $\Delta d/d \approx 4 \times 10^{-4}$) at room temperature and at 350°C, outside and within the furnace, respectively. A preliminary data reduction was performed, including merging of outputs from single counters in the bank and correction for detector efficiency as a function of neutron wavelength.

The Rietveld refinements of the β' and β crystal structures were performed by the GSAS computer package (9). Chebyshev polynomials of first kind with 14 (β') and 20 (β) coefficients were used to model the intensity background, and the peak shape was represented by a convolution of a pseudo-Voigt function (linear combination of Gaussian and Lorentzian compoents, with σ and γ half-widths, respectively: sample contribution) with two back-to-back exponentials (instrumental and moderator contributions) (10). Linear dependences of the σ and γ parameters on d_{hkl} were assumed: $\sigma = \sigma_1 d_{hkl}$, $\gamma = \gamma_1 d_{hkl}$. The mixing coefficient and the full width of the pseudo-Voigt function depend on σ and γ according to equations given in Ref. (11).

Starting from the atomic coordinates of the $P2_1/n$ structure of $Fe_2(SO_4)_3$ (12), the isotropic refinement of the β' phase converged successfully, and subsequent difference Fourier maps showed unambiguously the position of a single Li atom as the strongest negative peak (the neutron scattering length of Li is negative, unlike Zr, P, and O). This was included in the refinement, and convergence was attained with the agreement factors and unit-cell constants reported in Table 1. The refined weight fraction of the impurity phase ZrP_2O_7 was 6.4%. No evidence of disorder or partial occupancy of the lithium site was given by either the final difference Fourier map or the refinement of the Li occupation factor.

The structure of the phase was refined isotropically in the space group *Pbna* (standard orientation *Pbcn*), starting from

TABLE 1
Lattice Constants (with e.s.d's in Parentheses) and Rietveld Refinement Results for β-$LiZr_2(PO_4)_3$ (Space Group *Pbna*, $Z = 4$; $T = 350°C$) and β'-$LiZr_2(PO_4)_3$ ($P2_1/n$, $Z = 4$; $T = 20°C$)

	β-$LiZr_2(PO_4)_3$	β'-$LiZr_2(PO_4)_3$	α'-$LiZr_2(PO_4)_3$ (II)	α'-$LiZr_2(PO_4)_3$ (I)
a	8.84303(5) Å	8.81277(4) Å	8.8556 Å	15.0718 Å
b	8.94120(6)	8.94520(5)	9.1234	8.8556
c	12.41301(8)	12.37540(6)	12.5284	9.1234
α	90°	90°	86.730°	89.661°
β	90	90.801(1)	90.269	123.912
γ	90	90	90.429	90.429
V	981.463(8) $Å^3$	975.482(6) $Å^3$	1010.52 $Å^3$	1010.52 $Å^3$
Data	5039	3361		
Variables	71	98		
R_p	0.0345	0.0301		
wR_p	0.0429	0.0353		
$R(F^2)$	0.1007	0.0334		
χ^2	7.20	6.96		

Note. Data of triclinic α'-$LiZr_2(PO_4)_3$ from Ref. (3) are reported for comparison, referred to the original cell I ($C\bar{1}$) and to cell II ($I\bar{1}$), corresponding to that of the β' phase.

the coordinates of half the asymmetric unit of β'. Two negative peaks in general positions appeared clearly in the difference Fourier map, corresponding to feasible independent Li atoms with reasonable coordination environments. Their coordinates and occupation factors were refined by constraining the occupation factors to give a sum of 0.5, so as to contribute four Li atoms per unit cell and one per unit formula. The refinement converged (Table 1), but the displacement factors of Li1 and Li2 had to be kept fixed. The refined weight fraction of the impurity phase ZrP_2O_7 did not change significantly from the value obtained for the room-temperature phase, as expected, and it was thus kept fixed at 6.4% in the last cycles.

Experimental (including background), calculated, and difference profiles for both the β' and β phases are shown in Fig. 1. The same impurity peaks appear in both patterns. The quality of both fits (cf. Table 1) is similar and very satisfactory, as far as the fully profile agreement indexes (R_p, wR_p, and χ^2) are concerned, while the $R(F^2)$ value for Bragg intensities is not as good in the case of high-temperature experiment (β phase). This should be surely ascribed to the neutron absorption of the furnace metal walls, which does not affect the room-temperature results. Attempts to refine the absorption coefficient according to the GSAS routine failed because of high correlation with several refinement parameters. However, it should be taken into account that $R(F^2)$ values are usually larger than the corresponding full profile indexes R_p or wR_p in most Rietveld refinements, so that the $R(F^2) = 0.10$ value of the β phase is not bad at all on an absolute scale.

RESULTS AND DISCUSSION

Crystal Structures and Symmetry/Pseudo-symmetry Relations

The refined atomic coordinates and displacement parameters of β'- and β-$LiZr_2(PO_4)_3$ are reported in Tables 2 and 3, respectively. All atoms in the asymmetric unit of monoclinic β' are grouped in pairs (primed and unprimed) related by the pseudo-symmetry operation $x, 1/2 - y, -z$, except for $P2$, which lies close to the pseudo-special position $0, 1/4, 1/2$, and for Li, which alone violates the pseudo-symmetry. A corresponding pseudo-symmetrical arrangement is obviously observed by the PO_4 and ZrO_6 coordination polyhedra (Table 4). The average shifts for atomic pair with respect to the exact $x, 1/2 - y, -z$ operation are 0.024, 0.022, and 0.011 for the x, y, and z fractional coordinates, respectively, and they are clearly significant if compared to the corresponding e.s.d.'s. In Figs. 2 and 3, projections of the unit-cell content along [100] (with a shift of $z = 0.25$ for the origin) and [001], respectively, are shown.

The pseudo-twofold axis parallel to [100] is present as a true symmetry operator in the orthorhombic space group *Pbna*, of which $P2_1/n$ is a subgroup. The corresponding structure is adopted by the β phase of $LiZr_2(PO_4)_3$ stable at $T > 300°C$ (Figs. 4 and 5), and, at room temperature, for instance by $Li_{2.72}Ti_2(PO_4)_3$ (13). Thus, the $\beta' \leftrightarrow \beta$ phase transition is expected to have a displacive-ferroelastic character, and "single" crystals of the monoclinic β' phase should actually show polysynthetic twinning like in the case of $Li_3Fe_2(PO_4)_3$ (14). This scheme is confirmed by inspection of the refined atomic coordinates of the high-temperature β phase (Table 3), except for Li atoms which are considered in the section below. The asymmetric unit is substantially isostructural with half of that reported for the β' case in Table 2. Analogous results are observed for the geometries of the P and Zr coordination polyhedra (Table 5).

Lithium Order–Disorder and Mobility

In the β' structure, Li is fully ordered and located in a quite regular tetrahedral surrounding (Table 4), and it is the only atom not obeying the *Pbna* pseudo-symmetry. Therefore, its four-coordinated atoms (O2, O4, O5, O6) are overbonded with respect to their pseudo-symmetrical atoms (O2′, O4′, O5′, O6′), and thus they show significantly longer P–O and Zr–O distances. Lithium appears to be normally bonded to its oxygen neighbours, with slightly long Li–O bond distances (the sum of Li^+ and O^{2-} ionic radii is 1.95 Å for tetrahedral coordination (15)). The sum of bond valences of Li, computed according to $s_i = \exp[(1.466\text{-}r_i)/0.37]$, where r_i is the individual Li–O bond length (16), gives 0.89 e. As there are no empty neighboring sites available for hopping, a low mobility of the Li^+ ion and then a small ionic conductivity should be expected in the present phase. Its very high activation energy (0.91 eV) is therefore fully accounted for on structural grounds.

This scheme is consistent with the known structures of similar compounds containing three Li atoms per formula unit, $Li_3Fe_2(PO_4)_3$ (14), $Li_3Sc_2(PO_4)_3$ (14, 17), and $Li_3In_2(PO_4)_3$ (18), which are monoclinic $P2_1/n$ at room temperature. Upon transforming the unit cells and asymmetric units reported in the original papers appropriately, one can recognize that all these phases are isostructural with β'-$LiZr_2(PO_4)_3$, except for the two Li atoms out of three which are missing in the present structure. In particular, the Li(3) and Li1 atoms of the indium and iron compounds, respectively, are located in the same position as Li of our phase (Table 2). This result is important, because it was shown by Bykov *et al.* (14) that Li2 and Li3 in β'-$Li_3Fe_2(PO_4)_3$ (called α phase in the original paper) pass to a disordered state in the β-type high-temperature *Pbna* superionic phase (called γ by the authors), and they are thus believed to be responsible for the enhancement of lithium mobility, while Li1 should not be involved in this process. The Li location in β'-$LiZr_2(PO_4)_3$ being not particularly favorable for a high Li^+ mobility is confirmed by

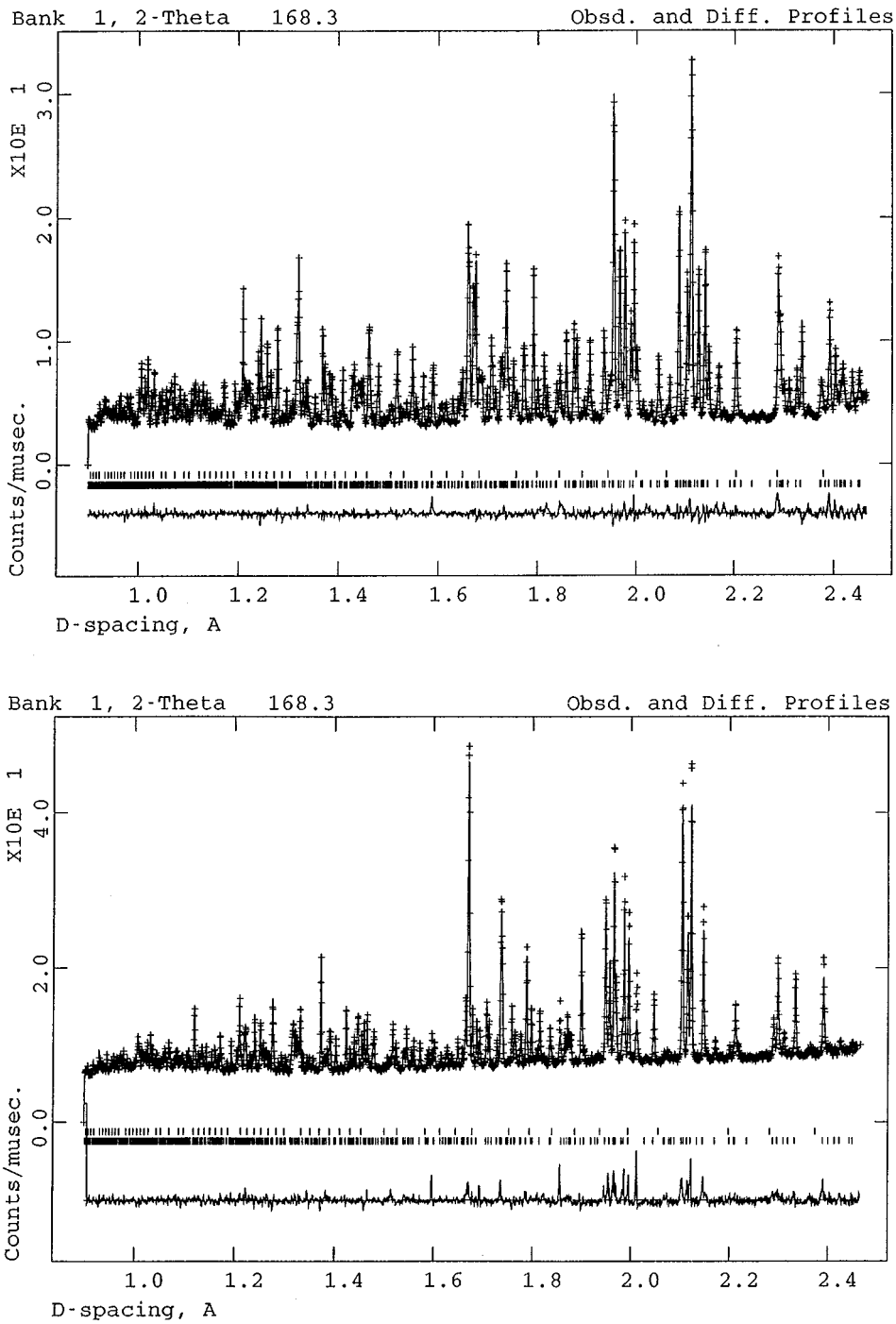

FIG. 1. Experimental (crosses), calculated, and difference profiles of the powder neutron diffraction patterns of β'-(above, 20°C) and β-(below, 350°C) $LiZr_2(PO_4)_3$.

comparison with α'-$LiZr_2(PO_4)_3$: there a much more distorted Li coordination tetrahedron is observed, and the average Li–O bond distance is larger (2.09 against 2.02 Å) than in the β' case, consistent with the higher ionic conductivity of the α' phase at room temperature (1).

As for the high-temperature β structure, lithium appears to be statistically distributed over two independent sites in the asymmetric unit (Table 3) and over four sites in the unit cell, which are symmetry-related in pairs. The refined occupancies of Li1 and Li2 give an approximate population

TABLE 2
Atomic Fractional Coordinates and Isotropic Displacement Parameters of β'-$LiZr_2(PO_4)_3$ ($P2_1/n$, $T = 20°C$)

	x	y	z	$U(10^{-2}$ Å$^2)$
Li	0.2946(13)	0.2229(12)	0.3279(9)	3.1(3)
Zr	0.7542(3)	0.4562(3)	0.6099(2)	0.86(7)
Zr′	0.7491(3)	0.0262(3)	0.3797(3)	0.84(7)
P1	0.6130(4)	0.1019(4)	0.6452(3)	0.96(9)
P1′	0.5976(4)	0.3808(4)	0.3539(3)	0.74(9)
P2	0.0351(4)	0.2514(5)	0.4901(3)	1.08(9)
O1	0.6505(4)	0.4191(4)	0.4666(3)	1.17(9)
O2	0.6789(4)	0.2552(3)	0.6796(3)	1.13(9)
O3	0.9479(4)	0.3628(4)	0.5581(3)	1.5(1)
O4	0.5729(4)	0.5941(4)	0.6575(3)	1.53(9)
O5	0.8319(4)	0.4837(4)	0.7721(3)	1.0(1)
O6	0.8435(4)	0.6639(3)	0.5776(3)	1.26(9)
O1′	0.6767(4)	0.0590(4)	0.5372(3)	1.54(9)
O2′	0.6259(4)	0.2143(4)	0.3318(3)	1.18(9)
O3′	0.9286(4)	0.1705(4)	0.4111(3)	1.48(9)
O4′	0.5588(4)	0.8931(4)	0.3562(3)	1.4(1)
O5′	0.8187(4)	− 0.0221(4)	0.2259(3)	1.1(1)
O6′	0.8807(4)	0.8583(4)	0.4353(3)	1.8(1)

Note. The e.s.d's are reported in parentheses. Corresponding primed and unprimed atoms are related by the pseudo-symmetry operation $x, 1/2 - y, -z$.

TABLE 4
Interatomic Distances (Å) and O–Li–O′ Angles (°) in β'-$LiZr_2(PO_4)_3$

Li–O2	2.097(12)	O2–Li–O4	106.5(5)
O4	2.018(11)	O2–Li–O5	82.2(4)
O5	2.001(11)	O2–Li–O6	100.0(5)
O6	1.979(12)	O4–Li–O5	133.0(6)
⟨Li–O⟩	2.024	O4–Li–O6	83.8(4)
		O5–Li–O6	141.5(6)
P1–O1′	1.506(5)	P1′–O1	1.504(5)
O2	1.546(5)	O2′	1.535(5)
O4′	1.514(5)	O4	1.524(5)
O5	1.546(5)	O5′	1.515(5)
⟨P1–O⟩	1.528	⟨P1′–O⟩	1.520
P2–O3	1.520(5)		
O6	1.563(5)		
O3′	1.528(5)		
O6′	1.532(5)		
⟨P2–O⟩	1.536		
Zr–O1	2.011(5)	Zr′–O1′	2.080(5)
O2	2.105(4)	O2′	2.084(5)
O3	2.014(4)	O3′	2.074(5)
O4	2.109(5)	O4′	2.074(5)
O5	2.126(5)	O5′	2.053(5)
O6	2.059(4)	O6′	2.013(4)
⟨Zr–O⟩	2.071	⟨Zr′–O⟩	2.063

Note. The e.s.d's are reported in parentheses.

ratio of 2 : 1. Li1 corresponds closely to Li in the β' case, but it is now disordered over two positions related by the [100] twofold axis ($x, 1/2 - y, -z$ operation), as occurs for Li2. The Li1 tetrahedral environment resembles that shown by Li in the low-temperature structure, yet with significantly longer Li–O distances (Table 5). Li2 shows a slightly more distorted but similar tetrahedral coordination and cannot be present locally together with a neighboring Li1 atom, as their shortest interatomic distance is only 1.56 Å. This short distance bridging partially occupied sites should

TABLE 3
Occupation Factors, Atomic Fractional Coordinates, and Isotropic Dispalcement Parameters of β-$LiZr_2(PO_4)_3$ (*Pbna*, $T = 350°C$)

	o.f.	x	y	z	$U(10^{-2}$ Å$^2)$
Li1	0.34(1)	0.2815(27)	0.2070(28)	0.3355(20)	2
Li2	0.16(1)	0.120(6)	0.145(6)	0.308(4)	2
Zr	1	0.7520(3)	0.4647(2)	0.6159(2)	0.73(5)
P1	1	0.6091(3)	0.1086(4)	0.6453(3)	1.16(8)
P2	1	0.0346(6)	0.25	0.5	1.8(1)
O1	1	0.6628(4)	0.4323(4)	0.4638(3)	2.61(9)
O2	1	0.6550(4)	0.2666(3)	0.6732(3)	2.21(9)
O3	1	0.9406(4)	0.3484(4)	0.5716(3)	2.44(9)
O4	1	0.5632(3)	0.5964(3)	0.6498(3)	2.03(9)
O5	1	0.8241(4)	0.4983(3)	0.7724(3)	1.77(8)
O6	1	0.8612(4)	0.6572(4)	0.5723(3)	2.34(9)

Note. The e.s.d's are reported in parentheses.

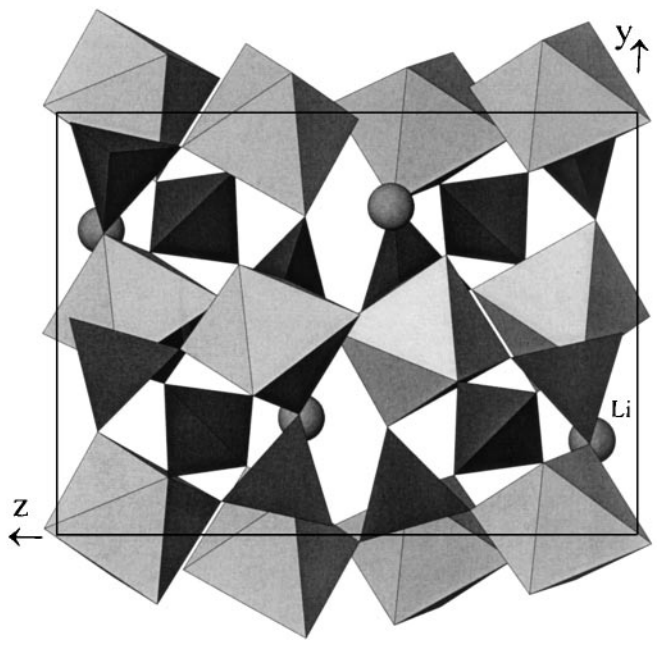

FIG. 2. Projection along [100] of the crystal structure of β'-$LiZr_2(PO_4)_3$. The origin is shifted by $z = 0.25$ with respect to coordinates in Table 2.

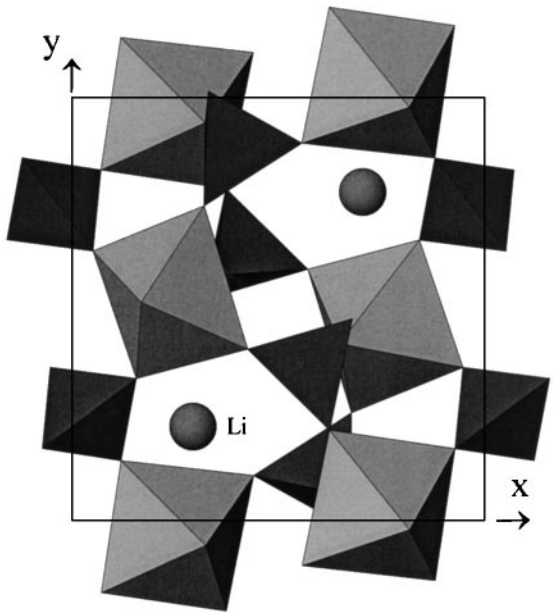

FIG. 3. Projection along [001] of half of the unit-cell content of β'-$LiZr_2(PO_4)_3$.

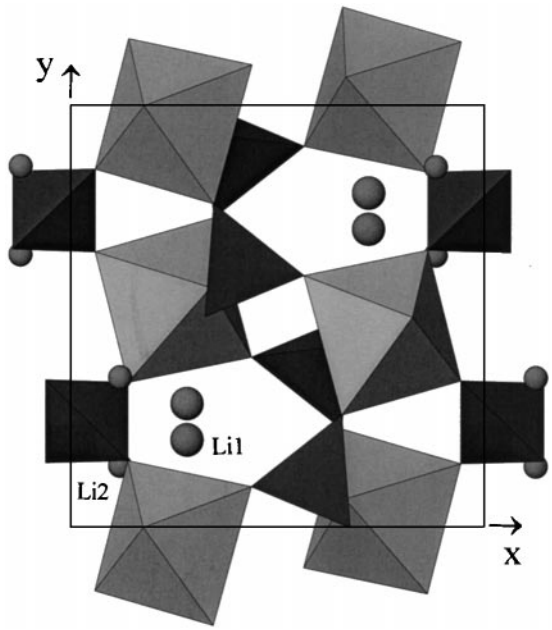

FIG. 5. Projection along [001] of half of the unit-cell content of β-$LiZr_2(PO_4)_3$.

produce a very low energy barrier for Li^+ ions jumping between the Li1 and Li2 positions. The sums of bond valences on Li1 and Li2 give 0.63 and 0.69 e, respectively, indicating a significant underbonding of both lithium sites which is consistent with low attempt frequencies in the hopping mechanism of ionic transport.

The second (3.53 Å) and third (4.14 Å) shortest Li–Li distances separate Li2 from Li1′ and Li1 from Li1″, respectively. Li1′ and Li1″ are related to Li1 by the $1/2 + x, y, 1/2 - z$ and $x, 1/2 - y, -z$ symmetry operations.

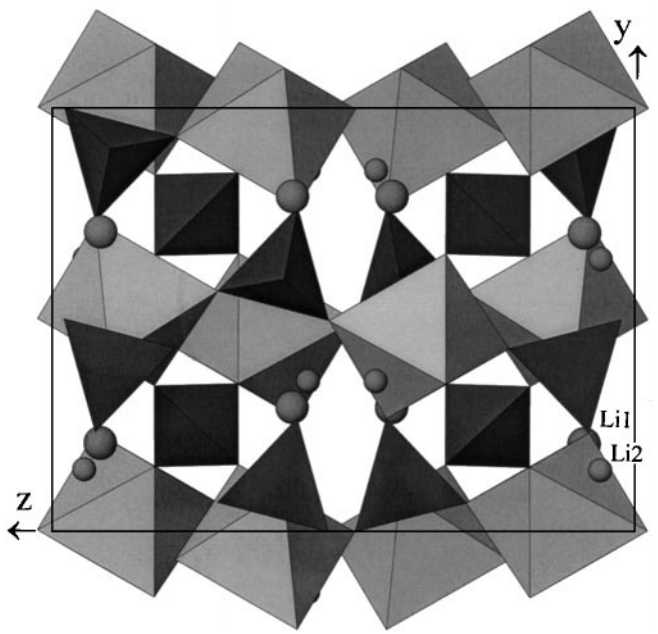

FIG. 4. Crystal structure of β-$LiZr_2(PO_4)_3$, projected along [100]. The origin is shifted by $z = 0.25$ with respect to coordinates in Table 3.

TABLE 5
Interatomic Distances (Å) and O–Li–O′ Angles (°) in β-$LiZr_2(PO_4)_3$

Li1–O2	2.317(26)	O2–Li1–O4	106.7(10)
O4	2.238(25)	O2–Li1–O5	81.1(9)
O5	2.032(25)	O2–Li1–O6	97.2(9)
O6	2.092(24)	O4–Li1–O5	128.9(12)
⟨Li1–O⟩	2.170	O4–Li1–O6	82.5(9)
		O5–Li1–O6	147.9(13)
Li2–O2	1.88(5)	O2–Li2–O3	136(3)
O3	2.18(6)	O2–Li2–O5	86(2)
O5	2.26(6)	O2–Li2–O6	104(3)
O6	2.31(6)	O3–Li2–O5	137(3)
⟨Li2–O⟩	2.16	O3–Li2–O6	66(2)
		O5–Li2–O6	120(2)
P1–O1	1.481(5)	Zr–O1	2.066(4)
O2	1.510(5)	O2	2.092(4)
O4	1.529(4)	O3	2.041(4)
O5	1.538(5)	O4	2.085(4)
⟨P1–O⟩	1.515	O5	2.066(4)
		O6	2.046(4)
P2–O3	1.502(5) × 2	⟨Zr–O⟩	2.066
O6	1.530(5) × 2		
⟨P2–O⟩	1.516		

Note. The e.s.d's are reported in parentheses.

Therefore, subsequent hoppings along the …–Li1′–Li2–Li1–Li1′–… pathway are able to propagate the Li^+ motion throughout the structure, with an activation energy determined by the larger energy barriers of the Li1–Li1″ and Li2–Li1′ steps. This mechanism explains the drop of activation energy observed at the $\beta' \leftrightarrow \beta$ phase transition.

By comparison with the high-temperature structure of $Li_3Fe_2(PO_4)_3$ determined at 300°C, it turns out that the present Li1 and Li2 positions roughly correspond to the analogous positions in that case (their atomic coordinates in our reference frame are 0.289, 0.218, 0.324 and 0.075, 0.087, 0.296, respectively). However, in that case the Li1 site has full occupancy, and Li2 has 0.25; furthermore, the Li1 to Li2 distance is larger than in β-$LiZr_2(PO_4)_3$ (2.19 against 1.56 Å), so that a direct transfer of Li^+ between the two positions seems to be less favored. The ionic conduction mechanism appears to be quite different, mainly because the third lithium site Li3 plays an important role (14) in $Li_3Fe_2(PO_4)_3$, but it is absent in the present case.

Relations with the α′/α NASICON-Type Phases

In order to understand the different coordination environments and mobilities of the Li^+ ion in the β' and α' polymorphs of $LiZr_2(PO_4)_3$, it is important to investigate the general crystal-chemical relationships between the two structures. First, the two lattices are quite similar, and the original α' unit cell (I) can be transformed into the β'-type unit cell (II) according to [010/001/101] (Table 1). The α' space group changes from $C\bar{1}$ to $I\bar{1}$. The most striking difference between the unit cells of the two phases concerns their volumes, as the α' cell is larger than the β' cell by 3.6%. We can thus expect a $\alpha' \rightarrow \beta'$ phase transition by applying pressure. Second, comparison of the [100] projections of the two structures (Figs. 2 and 6) shows strong similarities. We can recognize the presence of $c/2$ wide (001) slabs of PO_4 (T) and ZrO_6 (Oc) polyhedra, which are isostructural but differently stacked with respect to one another in the two phases. The Li atoms are located in hollows at the interface between pairs of adjacent layers. Each slab is built up by centrosymmetrical pairs of the typical NASICON unit Oc_2T_3, which are translated by the **a** and **b** lattice vectors (Fig. 3). Every Oc_2T_3 unit is characterized by a pseudo-symmetry twofold axis parallel to [100], so that the layer symmetry is $\bar{1}$, and the pseudo-symmetry is $2/b$. In the α' phase, adjacent slabs are related by a lattice translation, i.e., the centering vector $(\mathbf{a} + \mathbf{b} + \mathbf{c})/2$ of space group $I\bar{1}$. In the β' case, on the other hand, the relation between neighboring slabs is given by the *n* glide plane of space group $P2_1/n$ and by the *a* pseudo-glide plane of pseudo-symmetry *Pbna*. The latter way of packing layers is more efficient than the former method, leading to a smaller unit-cell volume and more compressed holes in the interlayer region where lithium can be accommodated. In both phases, neighboring layers are linked by sharing the O5 atoms between Zr octahedra and P1 tetrahedra, and O5′ between the Zr′ and P1′ polyhedra. Thus, only 2 out of 12 independent O atoms are involved in the interlayer linking, confirming the weaker character of this connection with respect to the intralayer linking.

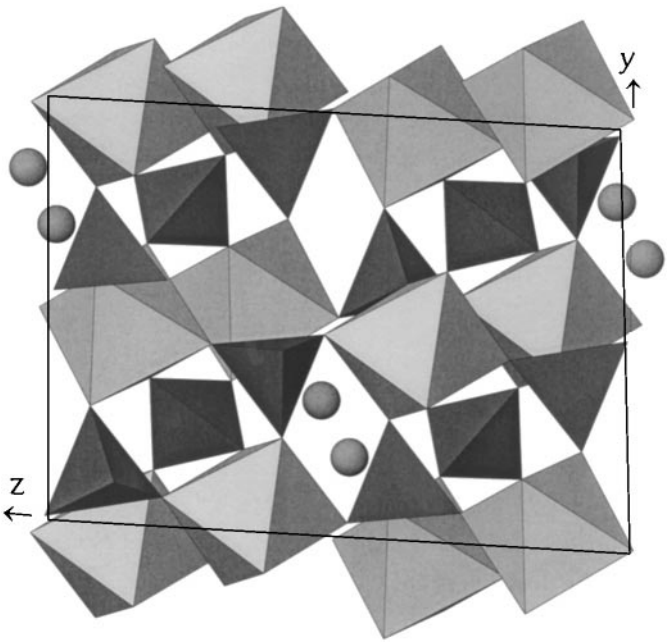

FIG. 6. Crystal structure of α'-$LiZr_2(PO_4)_3$, projected along [100]. The origin is shifted by $z = 0.25$ with respect to coordinates in Table 6 (cell II).

In order to show these structural relationships quantitatively, the asymmetric unit of the α' phase has been changed with respect to Ref. (3) and the corresponding atomic coordinates have been transformed consistently with the I to II unit-cell change, including an origin shift by 0, 1/2, 0: $x(\mathrm{II}) = y(\mathrm{I})$, $y(\mathrm{II}) = z(\mathrm{I}) - x(\mathrm{I}) + 1/2$, $z(\mathrm{II}) = x(\mathrm{I})$. The results are reported in Table 6. Upon comparing the transformed atomic coordinates (II) of the α' phase with the corresponding coordinates of β' (Table 2), the full similarity appears clearly for all but the lithium atoms. Therefore, we can conclude that the β' phase and the α' distorted NASICON structure differ just by the way symmetry relates the same layer-like structural unit. This is crucial, however, for the lithium environment and mobility in the interlayer region, because the Li^+ holes are significantly larger in the α' than in the β' case. Statistical distribution over two Li sites, longer ⟨Li–O⟩ distances, and larger ionic mobility ensue in the former with respect to the latter phase. Analogous results hold by comparing the corresponding high-temperature structures α and β.

CONCLUSIONS

The β' and β phases of $LiZr_2(PO_4)_3$, related by a reversible transition at 300°C, have been fully characterized

TABLE 6

Atomic Fractional Coordinates of α'-$LiZr_2(PO_4)_3$ (3), Referred to the Original Cell I ($C\bar{1}$) and to Cell II ($I\bar{1}$), Corresponding to That of the β' Phase

	x(I)	y(I)	z(I)	x(II)	y(II)	z(II)
Li1	0.726	0.022	0.412	0.022	0.186	0.726
Li2	0.714	0.900	0.314	0.900	0.100	0.714
Zr	0.6078	0.7525	0.5744	0.7525	0.4666	0.6078
Zr′	0.3921	0.7485	0.9390	0.7485	0.0469	0.3921
P1	0.6469	0.6066	0.2645	0.6066	0.1176	0.6469
P1′	0.3560	0.6084	0.2489	0.6084	0.3929	0.3560
P2	0.5074	0.0231	0.2554	0.0231	0.2480	0.5074
O1	0.4543	0.6922	0.3871	0.6922	0.4328	0.4543
O2	0.6589	0.6095	0.4375	0.6095	0.2786	0.6589
O3	0.5945	0.9292	0.4039	0.9292	0.3094	0.5945
O4	0.6276	0.5673	0.7231	0.5673	0.5955	0.6276
O5	0.7696	0.8062	0.7365	0.8062	0.4669	0.7696
O6	0.5607	0.8929	0.6901	0.8929	0.6294	0.5607
O1′	0.5377	0.6561	0.1088	0.6561	0.0711	0.5377
O2′	0.3320	0.6382	0.0625	0.6382	0.2305	0.3320
O3′	0.4332	0.9297	0.0914	0.9297	0.1582	0.4332
O4′	0.3399	0.5655	0.7640	0.5655	0.9241	0.3399
O5′	0.2450	0.8537	0.7530	0.8537	0.0080	0.2450
O6′	0.4279	0.8523	0.7743	0.8523	0.8464	0.4279

Note. Corresponding primed and unprimed atoms are related by the pseudo-symmetry operation $-x$, y, $1/2-z$ (cell I), or x, $1/2-y$, $-z$ (cell II).

structurally by powder neutron diffraction by determining the lithium positions and order–disorder states. In the high-temperature β structure, Li is disordered over four sites and related in pairs by a twofold symmetry axis. A full ordering of lithium occurs at the orthorhombic $\beta \rightarrow$ monoclinic β' phase transition, destroying the [100] twofold axis and leaving it as pseudo-symmetry, which relates all nonlithium atoms. Lithium is always in tetrahedral coordination, but with significantly longer Li–O bond distances in the disordered β structure. The sharp decrease of activation energy for Li^+ hopping, observed with the $\beta' \rightarrow \beta$ transformation, is accounted for by the passage from an ordered to a disordered state. This situation resembles that of the $\alpha' \rightarrow \alpha$ transition between NASICON-type phases of the same compound. In the latter case, however, the P–O–Zr slabs are stacked according to a simple translation, while in the former case they are stacked according to a glide reflection. It ensues that the interlayer hollows hosting lithium are larger in the α'/α than in the β'/β structures, improving the Li^+ ion mobility in the corresponding way.

ACKNOWLEDGMENTS

Financial support from M.U.R.S.T. and C.N.R. (Italy) is gratefully acknowledged. We thank Michele Finardi for his help with the synthesis and preliminary characterization of the phases studied in this work.

REFERENCES

1. F. Sudreau, D. Petit, and J. P. Boilot, *J. Solid State Chem.* **83,** 78 (1989).
2. M. Casciola, U. Costantino, L. Merlini, I. G. Krogh Andersen, and E. Krogh Andersen, *Solid State Ionics* **26,** 229 (1988).
3. M. Catti, S. Stramare, and R. Ibberson, *Solid State Ionics* **123,** 173 (1999).
4. M. Catti and S. Stramare, *Solid State Ionics*, in press.
5. A. D. Robertson, A. R. West, and A. G. Ritchie, *Solid State Ionics* **104,** 1 (1997).
6. V. Thangadurai, A. K. Shukla, and J. Gopalakrishnan, *J. Mater. Chem.* **9,** 739 (1999).
7. A. K. Padhi, V. Manivannan, and J. B. Goodenough, *J. Electrochem. Soc.* **145,** 1518 (1998).
8. Y. Sadaoka, Y. Sakai, M. Matsumoto, and T. Manabe, *J. Mater. Sci.* **28,** 5783 (1993).
9. A. C. Larson and R. B. Von Dreele, "GSAS: Generalized Structure Analysis System Manual." Los Alamos National Laboratory Report, LAUR: 86-748 (1994).
10. R. B. Von Dreele, J. D. Jorgensen, and C. G. Windsor, *J. Appl. Crystallogr.* **15,** 581 (1982).
11. P. Thompson, D. E. Cox, and J. B. Hastings, *J. Appl. Crystallogr.* **20,** 79 (1987).
12. P. C. Christidis and P. J. Rentzeperis, *Z. Kristall.* **141,** 233 (1975).
13. A. Wang and S. Hwu, *J. Solid State Chem.* **90,** 377 (1991).
14. A. B. Bykov, A. P. Chirkin, L. N. Demyanets, S. N. Doronin, E. A. Genkina, A. K. Ivanov-Shits, I. P. Kondratyuk, B. A. Maksimov, O. K. Mel'nikov, L. N. Muradyan, V. I. Simonov, and V. A. Timofeeva, *Solid State Ionics* **38,** 31 (1990).
15. R. D. Shannon, *Acta Cystallogr. Sect. A* **32,** 751 (1976).
16. I. D. Brown and D. Altermatt, *Acta Crystallogr. Sect. B* **41,** 244 (1985).
17. T. Suzuki, K. Yoshida, K. Uematsu, T. Kodama, K. Toda, Z. Ye, and M. Sato, *Solid State Ionics* **104,** 27 (1997).
18. D. Tran Qui and S. Hamdoune, *Acta Crystallogr. Sect. C* **43,** 397 (1987).